Boundary-Layer Meteorology
https://doi.org/10.1007/s10546-023-00819-9

RESEARCH ARTICLE

Turbulence in the Mixed Layer Over an Urban Area: A New York City Case Study

Gabriel Rios[1] · **Prathap Ramamurthy**[2]

Received: 7 January 2023 / Accepted: 13 June 2023

Abstract
This study examines the turbulence characteristics of the boundary layer over New York City. Understanding the urban boundary layer characteristics is key to forecasting weather in cities, where most people live. Although extensive research into urban boundary layer (UBL) processes have been carried out in the past decades, majority of these studies focused on the urban surface layer; our understanding of urban mixed layer characteristics is still incomplete. Here we use Doppler lidar observations from multiple sites in New York City to study turbulent properties in the UBL and their relationship to the heterogeneous urban surface. All three sites were influenced by different levels of urbanization. By investigating turbulent properties such as velocity variances, turbulent intensities, and vertical velocity spectra throughout the UBL, our analysis shows vertical stratification in momentum transport during non-neutral stability periods. The spectral analysis of vertical velocities show vertical stratification in normalized energy density at different heights, with the degree of stratification increasing with increasingly non-neutral surface stability. A comparison of turbulent properties over the study sites reveals a degree of homogeneity in mixed layer characteristics, with similar vertical profiles of the turbulent characteristics among the sites, suggesting horizontal homogeneity in the urban mixed layer.

Keywords Urban climate · Mixed layer · Atmospheric stability · Doppler lidar

1 Introduction

Mean spatial and temporal characteristics of the urban boundary layer (UBL) have been well-defined in the literature. Roth (2007) provides a detailed description of the vertical structure of the UBL by defining distinct sublayers of the UBL from the lowest (urban canopy layer) to the highest (mixed layer). In the urban canopy and roughness sublayers,

✉ Gabriel Rios
gabriel.rios@princeton.edu

Prathap Ramamurthy
pramamurthy@ccny.cuny.edu

1 Program in Atmospheric and Oceanic Sciences, Princeton University, Princeton, NJ, USA

2 Department of Mechanical Engineering, CUNY City College, New York, NY, USA

Published online: 24 August 2023

the influence of roughness elements dominate turbulent transport and the length scales of turbulent eddies (Kastner-Klein and Mathias 2004; Macdonald 2000), leading to a high degree of spatial heterogeneity. This phenomenon has been captured largely using high-frequency sonic anemometer data mounted at various heights on sizable roughness elements at multiple points within the same urban area, such as tall buildings (Hanna et al. 2007) and dedicated instrument towers (Nordbo 2013; Roth and Oke 1993; Wang et al. 2014). Above the roughness sublayer lies the inertial sublayer, within which flow properties become horizontally homogeneous and Monin-Obukhov similarity theory can be applied (Castillo et al. 2011; Rotach 1999).

The uppermost and deepest sublayer of the UBL is the mixed layer, which links surface and free atmosphere processes. The mixed layer is arguably the least understood of the sublayers due to observational constraints (Barlow 2014; Roth 2007; Wood et al. 2010). Mixed layer dynamics are complex and variable with height, although less is known with regards to spatial heterogeneity in the horizontal due to the influences of the surface layer. These dynamics lead to mixing, which is a result of turbulent flow that is driven by thermals, wind shear, and entrainment at the UBL interface with the free atmosphere. These processes are critical for transport of scalars, which lead to implications for qualities directly relevant to human interests (Baklanov et al. 2011; Barlow 2014; Klein et al. 2014). From a public health perspective, an improvement in understanding turbulent processes may lead to improved air quality forecasts and more precise modeling of heat risks on local scales (Garratt 1994; Petäjä 2016) However, the difficulty of observing the UBL at these heights has hindered the understanding of these turbulent processes, and within a context relevant to urban areas, how turbulence varies spatially within the UBL.

Various studies documenting and analyzing observational data have made significant progress to address the gaps in this field. Early campaigns to collect observations of the mixed layer used measurements taken aboard aircraft to collect data, from which turbulent quantities throughout the depth of the boundary layer could be derived (Hildebrand and Bernice 1984; Lenschow et al. 1980). Such campaigns provided some of the first estimates for turbulent kinetic energy (TKE) budget terms and other second-moment turbulence budgets, which has been influential for numerous studies in observations of turbulent processes and modeling of turbulence in the boundary layer. The drawbacks of these methods were somewhat addressed by the use of tall towers (exceeding 30 m) in urban areas, upon which multiple instruments were mounted at different heights to provide data from longer observational periods, enabling for analysis of the surface and lower mixed layer over a range of meteorological conditions (Roth 1993; Roth and Oke 1993; Feigenwinter et al. 1999). In (Roth 1993) and (Roth and Oke 1993), comprehensive observations led to a broad suite of spectral and integral statistical data analyzing turbulence over an urban area at novel heights. Findings reported in Feigenwinter et al. (1999) performed similar analyses with a well-instrumented tall tower up to 76 m AGL, enabling comprehensive vertical profiles of turbulent characteristics over a range of stability regimes. These efforts were significant in the advancement in understanding processes above the surface layer and into the inertial sublayer and lower mixed layers over urban areas, although they were unable to capture turbulent processes at greater heights. These constraints were addressed in novel efforts to implement Doppler lidar for measuring winds through the depth of the boundary layer, with studies showing the ability of Doppler lidar to resolve wind at high spatial and temporal resolutions at unprecedented heights, indicating the ability to resolve low-frequency turbulent features in the mixed layer (Collier et al. 2005; Newsom et al. 2005). More in-depth evaluation of turbulence in the mixed layer over urban areas was made possible using lidar and supertall towers that allowed for extended observation periods at high frequencies, resulting in the ability to analyze turbulent mixing

throughout the boundary layer and its relation to surface layer fluxes (Quan and Fei 2009a; Wood et al. 2010), as well as boundary layer characteristics during a range of conditions, including cloud-topped boundary layer and nocturnal low-level jet events (Barlow et al. 2011; Hogan et al. 2009). More recently, measurements deeper into the mixed layer in urban areas have expanded to capture a wider range of turbulent phenomena over smaller timescales, ranging from observations of turbulent and scalar transport under a range of surface stability conditions (Wang et al. 2014), to analyses of the daily and intra-city variability of pollutant dispersion, (Kotthaus 2018), and the evolution of the morning boundary layer (Halios and Janet 2018).

Despite extensive efforts made to answer open questions regarding turbulence in the UBL, our understanding is still emerging, particularly in the mixed layer. Understanding these characteristics is essential because turbulent processes in the boundary layer connect local phenomena to synoptic-scale conditions, rendering increased value to observations for the improvement of weather and air quality forecasting efforts (Morss 2011; National Research Council et al 2012). New York City presents a particularly complex case for studying the UBL, as the combination of multiple sea breeze fronts from Long Island Sound and the New York/New Jersey Bight and localized flows generated by the effects of heterogeneous surface properties over a large area can result in a strongly-modified dynamic and thermodynamic structure relative to other urban areas studied in the literature (Banks et al. 2015; Barlow 2014; Calmet and Mestayer 2016; Haman et al. 2012). Although numerous studies have performed detailed modeling of turbulent processes or extended observations of boundary layer profiles (e.g., winds, temperature, moisture), few have observed and analyzed turbulent processes in the mixed layer over urban areas.

The observations and analysis presented herein are an attempt to improve our understanding of turbulence over a large coastal urban area with highly variable surface properties and, due to its geographical setting, complex mesoscale meteorology. We are particularly focused on the following scientific questions:

1. What are the mean and turbulent characteristics of the UBL for a large urban area?
2. How does boundary layer turbulence vary spatially within a large urban area?
3. How much do surface layer characteristics influence the mixed layer?

2 Data and Methods

2.1 Observation Sites

The observation sites are shown in Fig. 1 overlaid on land cover type and building height, respectively. Measurements were taken at 3 sites within New York City between September 2020 and August 2021 in the boroughs of Manhattan, Queens, and Staten Island (see Table 1). The Manhattan site is located on the campus of The City College of New York in Harlem, which is highly urbanized and generally consists of mid- and high-rise residential buildings (maximum of 65 m per zoning regulations (NYC 2023)). Prominent geographical features include the Hudson River approximately 800 m to the west and St. Nicholas Park, which presents a narrow area of vegetated surfaces, directly to the east. The Queens site is located on the campus of Queens College in Flushing, which is also highly urbanized and generally consists of low- and mid-rise residential buildings (maximum of 32 m per zoning regulations (NYC 2023)). Flushing Meadows-Corona Park, which features large vegetated areas, is located due west of the site. The Staten Island site is located on the campus of the

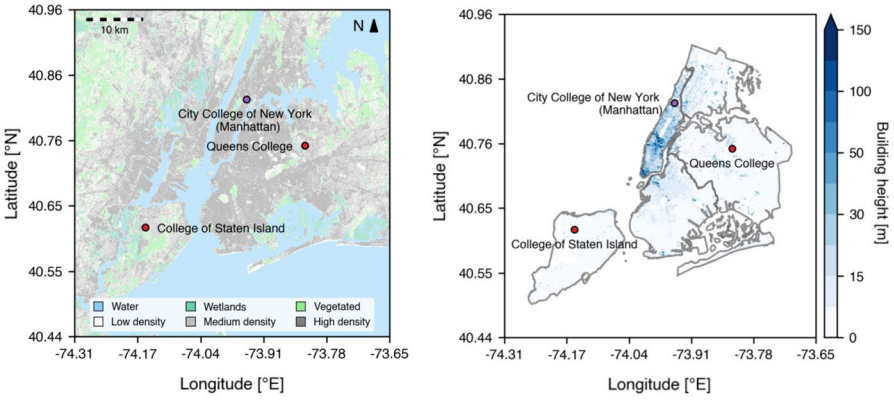

Fig. 1 **a** Map of observation sites and **b** building heights in New York City (approximately 50 m resolution). Locations within the NYS Mesonet are identified with a red dot, whereas independent locations are identified with a purple dot

Table 1 Information regarding observation sites and periods

Site	Coordinates	Elevation (m a.g.l.)	Area-averaged building height (z_H) (m a.g.l.)	Observation period
Manhattan	40.8216° N, −73.9474° E	35.9	10.0	15 Jul 2021 to 01 Sep 2021
Queens	40.7343° N, −73.8159° E	25.6	5.82	01 Sep 2020 to 01 Sep 2021
Staten Island	40.6040° N, −74.1485° E	8.90	4.58	01 Sep 2020 to 01 Sep 2021

College of Staten Island and is surrounded by low-rise residential buildings in the greater vicinity (maximum of 10.7 m per zoning regulations (NYC 2023)). The campus presents a mixture of low-rise buildings, open vegetated surfaces, and a small woodland area due west, with urbanized areas immediately surrounding the campus. The variation of building classes, degree of urbanization, and surface types presents a range of conditions characteristic of New York City (Table 2).

2.2 Observational Instruments

2.2.1 Doppler Wind Lidar

Measurements of wind velocity were made using a network of Vaisala/Leosphere WindCube Doppler wind lidars, with WindCube 100 S lidars deployed at the Queens and Staten Island sites as part of the New York State Mesonet (Shrestha et al. 2021) and a WindCube 200 S lidar installed atop Steinman Hall on the City College of New York campus in Manhattan. The WindCube 100 S operated in Doppler beam swinging (DBS) mode, allowing for 3-dimensional wind measurements in the four cardinal directions at an elevation angle of 75°, with a scan cycle lasting approximately 20s (Shrestha et al. 2021). The WindCube 200 S operated in vertical stare mode throughout the duration of the observation period, allowing for retrieval of the vertical component of the wind velocity. The vertical stare mode was chosen over the DBS mode to obtain a higher sampling rate, allowing for improved reso-

Table 2 Instrument parameters for the Vaisala/Leosphere WindCube lidar network

Parameter	100 S	200 S
Wavelength	1.54 μm	1.54 μm
Pulse repetition frequency	20 KHz	20 KHz
Pulse length	50 m	50 m
Integrated signal frequency	0.20–0.25 hz	1 hz
Vertical range	0.1 to 7.0 km	0.1 to 7.0 km
Vertical resolution	100 m	100 m
Scan configuration	DBS	Vertical stare
Wind components measured	u, v, w	w

lution of vertical wind velocity (w). The WindCube 100 S lidar data was obtained every 4 to 5s for each component in DBS mode, whereas WindCube 200 S lidar data was obtained every second in vertical stare mode. Data with signal-to-noise ratio (SNR) values below −22 dB and data obtained during precipitations events were rejected. It is worth noting that significant amounts of data above 1.5km were rejected by imposing this threshold, although this varied with time of day (more data availability at greater heights during the day), which appears to be a function of boundary layer height, as noted in Kumer et al. (2014); Wang et al. (2016). Measured quantities were detrended every 3 min with the objective of ensuring mean and fluctuating values representative of the time periods during which they were recorded. Detrended data were then binned into 30 min groups used for computation of turbulent quantities (such as wind variances and velocity spectra), similar to practices outlined in Foken et al. (2004). Additional removal of outliers (≥ 3–σ) was performed per 30 min group. Availability of lidar data as a percentage of 30 min intervals per month are listed in Table 3. With regards to the data availability in Manhattan, data prior to July 2021 was not available either due to instrument installation in January 2021 and lack of access to data until July 2021. This data was included with the data from the Queens and Staten Island sites to allow for comparison of observations from overlapping time periods, although availability of the Manhattan data from September 2020 to July 2021 would significantly benefit this study (additional discussion is provided in Sect. 4). Additional technical specifications for both instrument models are provided in Table 2.

Doppler lidars operated by the New York State Mesonet (corresponding to Queens and Staten Island locations) were also used to estimate mixing layer height (z_i), based on the maximum vertical gradient in aerosol concentration as detected by lidar and corroborated with radiosonde data from the nearest National Weather Service office and numerical weather prediction data (Granados-Muñoz et al. 2012; Shrestha et al. 2021). Although the lidar data from the Manhattan site is not used to estimate z_i, estimates for z_i in Manhattan are generated by averaging data from Queens and Staten Island sites given the homogeneity in mixed layer heights between sites within the same urban area, at considerable distance from the rural–urban interface such that UBL height is relatively spatially-invariant within the urban area (Godowitch et al. 1978; Mestayer et al. 2008; Pal 2012).

2.2.2 Surface Flux Stations

Surface parameters, such as 2 m air temperature, short- and longwave radiation, and wind velocity at high temporal resolutions (10 hz), were measured by surface flux stations at each site. These parameters were used to derive friction velocity (u_*), atmospheric stability (ζ), and the convective velocity scale (w_s^*), all of which are relevant for classifying and normalizing

Table 3 Lidar data availability percentage per month per site. Table cells with no entry indicate no data is available for the site during the corresponding month

	2020				2021							
	Sep	Oct	Nov	Dec	Jan	Feb	Mar	Apr	Mar	Jun	Jul	Aug
Manhattan											9	31
Queens	32	26	38	36	45	42	32	54	54	61	57	46
Staten Island	70	51	48	37	18	55	62	77	78	83	82	77

turbulent parameters in this study. At Queens and Staten Island, the New York State Mesonet operates flux stations using a sonic anemometer (v200A, G. Lufft Mess- und Regeltechnik GmbH) to record wind speeds and direction at an output frequency of 1 hz. At Manhattan, the City College of New York operates a sonic anemometer (IRGASON, Campbell Scientific) to record wind speeds and direction at an output frequency of 10 hz. For the purposes of this study, only measurements from the sonic anemometer were used. Turbulent quantities (e.g., standard deviations of wind components) and fluxes were calculated from 10 hz data. Quality checks were then applied to the data, with data rejection for periods when instrument diagnostic flags indicated an instrument or program error and outlier removal using a 3-σ threshold relative to the 30 min average to remove spikes. The effects of surrounding structures were also taken into account during quality filtering, as the Manhattan and Queens sites have structures in proximity to the anemometers that may affect measurements. To reduce the impact of building effects on measurements, data corresponding to surface wind directions with a northerly component at the surface ($\phi \leq 90°, \phi \geq 270°$) was omitted for Manhattan and with an easterly component at the surface ($0° \leq \phi \geq 180°$) was omitted for Queens. It is worth noting that the lowest vertical lidar levels exceed $10z_H$ (area-averaged building height) for each site, indicating that building effects on lidar observations are negligible. Therefore, directional filtering is not applied for lidar data.

2.3 Analytical Methods

2.3.1 Stability Classification

Atmospheric stability at the surface is used to observe UBL processes under different convective regimes and is chosen for grouping of observations over time-of-day, as we are interested in observing turbulence as a function of convective activity, which is related to, although not fully dependent, on time of day. Atmospheric stability (ζ) is calculated at each site as $\zeta = z/L$, where z is the observation height minus the zero-plane displacement height (z_d) and L is the Obukhov length, which is calculated as $L = -\overline{\theta_v} u_*^3 / \left(kg(\overline{w'\theta_v'})_s\right)$ (Stull 1988). In this expression, θ_v is the potential virtual temperature (approximated by sonic temperature, T_s) and u_* is the friction velocity as calculated by $u_* = \left(\overline{u'w'} + \overline{v'w'}\right)^{1/4}$ at the surface. Parameters relevant for calculating ζ are measured by the surface flux stations and/or sonic anemometers at each location, with ζ values being derived at 30 min intervals. For the purpose of this study, ζ is classified into 5 groups ranging from most to least convectively active: highly unstable ($\zeta < -0.5$), unstable ($-0.5 \leq \zeta < -0.1$), neutral ($-0.1 \leq \zeta < 0.1$), stable ($0.1 \leq \zeta < 0.5$), and highly stable ($\zeta \geq 0.5$). It is emphasized that the stability calculated herein is local relevant to each observation station.

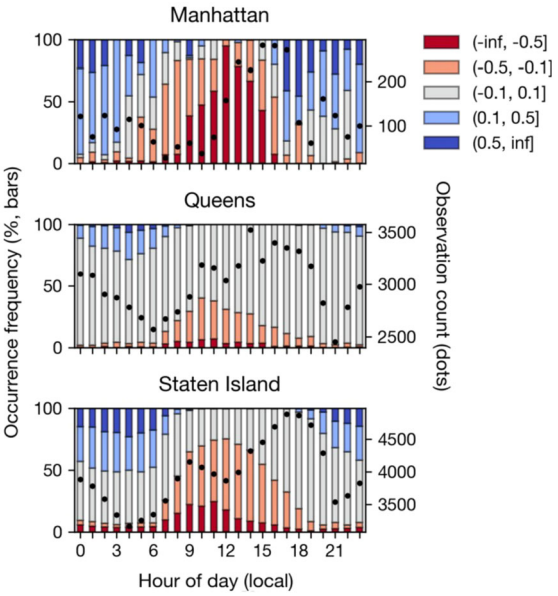

Fig. 2 Composite diurnal mean occurrence fraction of surface stability at the observation sites, categorized into highly unstable ($\zeta < -0.5$), unstable ($-0.5 \leq \zeta < -0.1$), neutral ($-0.1 \leq \zeta < 0.1$), stable ($0.1 \leq \zeta < 0.5$), and highly stable ($0.5 \leq \zeta$) conditions. The black dots show the observation count for each hour

2.3.2 Velocity Spectra Generation

Velocity spectra are computed herein to determine the peak frequencies for various surface stability regimes at different heights in the surface and mixed layers, the latter of which has not been reported in the literature, to the authors' knowledge. Velocity spectra are generated at Manhattan using 1 hz vertical stare lidar data for w. It is worth noting that only Manhattan data is used for spectral analysis due to its higher temporal resolution relative to Queens and Staten Island (≤ 0.25 hz), which may fail to resolve smaller or more transient flow features, especially those in the high-frequency end of the inertial subrange and beyond (Cheynet et al. 2018; Grachev et al. 2013). A fast Fourier transform (FFT) algorithm was used to derive spectra for w, with a filter to remove outliers ($\geq \pm$ 3-σ) and window-averaging (128 frequency windows) being performed on spectra over the range of resolved frequencies to filter out anomalous values. Normalization of the spectral frequencies and spectral energy density were then performed; spectral frequencies (f) were normalized by multiplying by the quotient of the vertical level of observation (z) by 30 min-averaged horizontal winds (U) at that vertical level, whereas the spectral energy density was derived by multiplying the spectra (S_w) by the quotient of their corresponding frequencies (f) and the square of U at the vertical level of observation (Stull 1988).

3 Results and Discussion

3.1 Mean Flow Characteristics of the UBL

This study will group UBL phenomena by surface stability instead of time of day, as surface stability is generally a better predictor for UBL properties than time of day. To demonstrate surface stability as a function of time of day, the composite diurnal occurrence frequency of

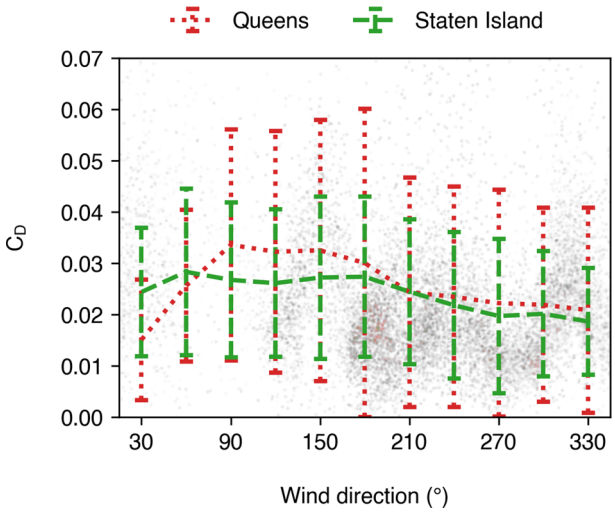

Fig. 3 Drag coefficients (C_D) at the Queens and Staten Island observation sites taken during neutral surface stability ($-0.1 \leq \zeta < 0.1$) conditions, as a function of wind direction (in degrees). Scatter plots show individual points, while error bars show mean and $\pm$ 2-σ values

different local surface stability regimes is shown in Fig. 2. The composite diurnal occurrence frequency is calculated by dividing (a) the number of 30 min observation periods for each stability regime in the corresponding hour by (b) the total number of 30 min observation periods in the corresponding hour. For all sites, the diurnal profile of surface stability is apparent; early morning and late night hours are predominantly neutral or stable, whereas daytime hours are predominantly neutral or unstable. Stability distributions from Manhattan are skewed unstable relative to the other sites due to a smaller sample size with observations taken from summer months only. Highly unstable periods occur most frequently during the morning hours, which indicates the occurrence morning transition period and the growth of the mixed layer (Halios and Janet 2018). Throughout the day, local stability gradually becomes less unstable as the boundary layer reaches its peak height and vertical mixing is strongest.

The drag coefficient, C_D, is used to estimate the effects of roughness elements upwind of the sites and to help establish the degree of similarity of the observational locations to those in similar studies of UBL turbulence. Estimates of C_D were made using the relation $C_D = (u_*/\overline{U})^2$, where $\overline{U}$ is the average horizontal wind speed over the 30 min period. These estimates were generated during near-neutral ($-0.1 \leq \zeta \leq 0.1$) conditions at the elevation heights listed in Table 1, with results for Queens and Staten Island over the observation period shown in Fig. 3 (Manhattan data excluded due to small sample size during near-neutral conditions). The Queens location shows higher mean values of C_D than Staten Island over all wind directions, ranging from 0.005 from northerly winds ($\phi \geq 315°$ and $\phi \leq 45°$) to 0.04 from easterly winds ($45° \leq \phi \leq 135°$), whereas Staten Island mean values range from 0.004 during southwesterly ($180° \leq \phi \leq 270°$) winds to 0.01 during southeasterly winds ($90° \leq \phi \leq 180°$). This aligns with measurements from studies in other urban areas, such as those from rooftops in midtown Manhattan (0.01 to 0.09), downtown Oklahoma City (0.03 to 0.05) (Hanna et al. 2007) and central London (0.004 to 0.008) (Wood et al. 2010).

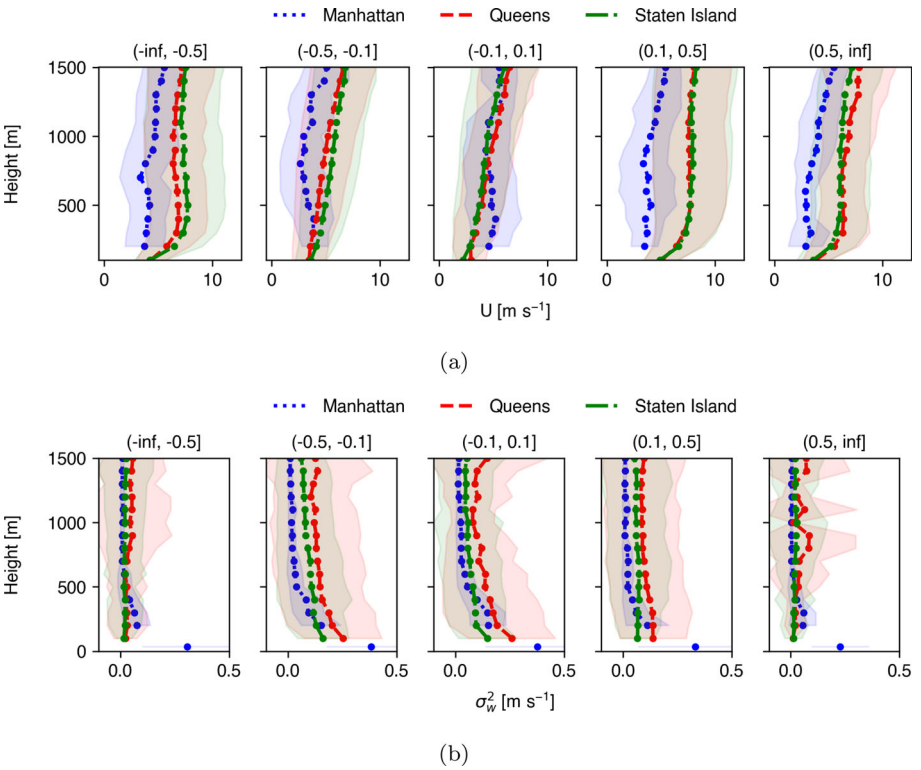

Fig. 4 Vertical profiles of **a** mean horizontal wind and **b** variance of vertical velocity, averaged by stability group. Shading indicates $\pm$ 2–σ from the mean over the observation period

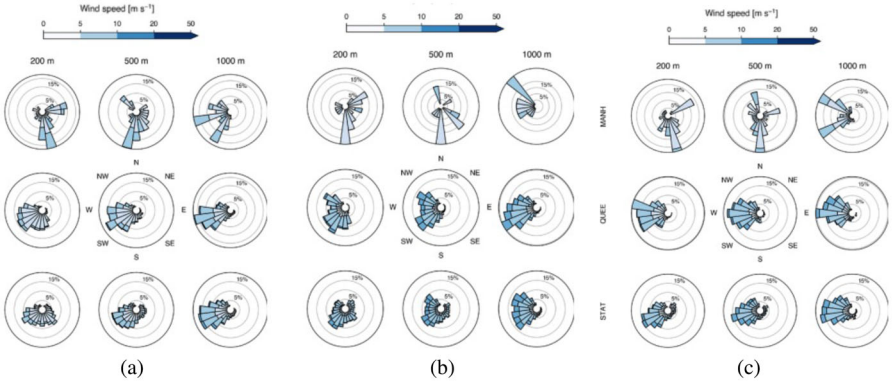

Fig. 5 Wind roses showing composite mean wind direction, wind direction frequency percentage, and the corresponding wind speeds at Manhattan, Queens, and Staten Island sites during **a** unstable ($\zeta < -0.1$), **b** neutral ($-0.1 \leq \zeta < 0.1$), and **c** stable $\zeta \geq 0.1$ regimes

The vertical profiles of mean horizontal wind U and variance of vertical velocity σ_w^2 are shown in Fig. 4, while wind directions are shown in Fig. 5 for unstable, neutral, and stable categories. Vertical profiles of U are similar over Queens and Staten Island, with logarithmic profiles during unstable and stable periods and more linear profiles during neutral conditions. In contrast, Manhattan exhibits a less stratified vertical profile of U with lower $\partial U/\partial z$ relative to Queens and Staten Island, especially during unstable periods. For all sites under all stability regimes, mean values of U remained below 10ms^{-1}. This is suggestive of the formation of a local internal boundary layer as a response to an increase in roughness heights in Manhattan relative to other boroughs, resulting in lower horizontal wind speeds and a shift in wind direction at lower levels (Garratt 1990; Kaimal and Finnigan 1994; Verkaik and Holtslag 2007; Melecio-Vázquez et al. 2018). With regards to differences in wind speeds between regimes, Fig. 5 shows a higher frequency of stronger horizontal winds with increasing local stability. A potential phenomenon behind this trend is the presence of nocturnal low-level jets over the mid-Atlantic United States, which often occur in the early morning during stable periods (Delgado 2015; Sullivan 2017; Zhang et al. 2006). Winds are primarily out of the southwest over all stability categories, with winds becoming increasingly westerly with height towards the top of the boundary layer. Additionally, wind directions during neutral periods exhibit more variability relative to stable and unstable periods.

Averaged vertical profiles of vertical velocity variance, or σ_w^2, are also shown in Fig. 4 which are being shown to demonstrate the variability of w, which is more relevant for insights on turbulent mixing than mean values of w. Low-level σ_w^2 ranges from values ranging from $0.35\text{m}^2\text{s}^{-2}$ at 200 m above ground level (AGL) during unstable periods to $0.21\text{m}^2\text{s}^{-2}$ during stable periods. It is worth noting that values are near-zero during highly unstable ($\zeta < -0.5$) and highly stable ($\zeta > 0.5$) periods throughout the boundary layer above the surface, despite ranging from 0.38 to 0.22 at the surface in Manhattan. With regards to other periods, mean values of σ_w^2 exhibit similar behaviors to vertical profiles of different boundary layer properties (such as horizontal wind speed) . Specifically, this behavior is characterized by higher values near the surface and lower values throughout the mixed layer, which eventually become constant with increasing height. The magnitude of σ_w^2 decreases at lower levels with increasing stability, which is expected given that vertical mixing is weaker during less convective periods. With regards to lower than expected σ_w^2 values during highly unstable periods, the near-zero σ_w^2 values throughout the UBL during highly unstable periods occur during the morning transition, which may be a result of near-surface heating not yet having mixed vertically to height. This is similar to findings for observations over London (Halios and Janet 2018).

3.2 Turbulent Intensity

Figure 6 shows the turbulence intensity $[I_j = \sigma_j/\overline{U},\ j = (u, v, w)]$ grouped by stability for the zonal (u), meridional (v), and vertical (w) directions over heights normalized by mixed layer heights (z_i) corresponding to individual observations. In this definition, σ_j is the standard deviation of winds. During unstable periods ($\zeta < -0.1$), mean zonal turbulent intensity I_u values range from 0.2 to 0.7 over the height of the mixed layer, with values remaining somewhat constant from the surface layer to the top of the mixed layer, with the exception of values in Manhattan peaking near-surface. For reference, these values align with mean values of $\sigma_u/\overline{U}$ from rooftops in midtown Manhattan observed by Hanna et al. (2007) ranging from 0.3 to 0.6 during slightly unstable conditions. Higher values are also observed during stable periods $z/z_i < 0.5$, with I_u averaging between 0.3 and 0.44 in Queens and

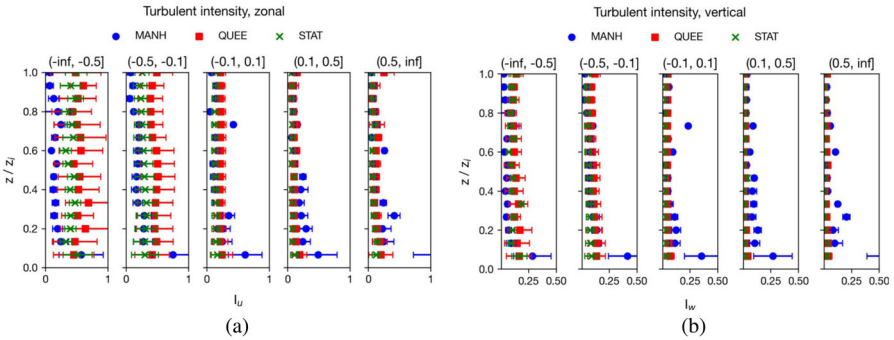

Fig. 6 Turbulent intensity profiles over heights normalized by boundary layer height for **a** zonal and **b** vertical directions, grouped by stability

Staten Island. During near-neutral stability periods, the I_u values exhibit a more logarithmic vertical structure, with decreasing I_u with increasing height. In addition to the mean I_u values, the variability (as shown by the error bars) is small relative to the mean values during these periods, and variability during stable periods is expectedly lower than during unstable periods.

Mean vertical turbulent intensity values (I_w) follow a similar trend as I_u with respect to stability, as I_w decreases with increasing stability. Additionally, I_w is highest near the surface, with all sites reporting similar mean values during highly unstable periods (0.2 to 0.3) with progressively lower values as ζ increases (typically ≥ 0.15). Moreover, the vertical gradient of I_w is generally low throughout the rest of the mixed layer, with the exception of a slight positive gradient at $z/z_i = 1$ during unstable periods, suggesting some mixing with the free atmosphere at the top of the boundary layer.

In analyzing the turbulent intensity profiles, several inferences can be made. The relatively high values of I_j observed during the unstable periods are likely caused by the joint influence of thermally- (high buoyancy at lower z/z_i) and mechanically-induced (high shear at higher z/z_i) turbulence due to high and unevenly distributed surface roughness, which will increase σ_j. Lower values of I_j observed during periods of near-neutral stability can be attributed to the collapse of the boundary layer. During stable periods, high values of low-level I_j are likely due to intermittent shear-generated turbulence, which may result in the variability of u and w (larger σ_j) without a similar effect on mean values. This is especially noticeable for the Manhattan site, which consistently has higher near-surface mean and standard deviation values of I_w than the other sites, especially during stable periods. This implies the effect of shear-generated turbulence downstream of roughness elements surrounding the observation site from taller buildings than present around the other sites, which is suggested by Manhattan having the largest area-averaged building height (Table 1).

To determine how observations of I compare with data from the literature, we overlay data from Roth (2007) over the inertial sublayer and lower mixed layer as shown in Fig. 6. The black curves in the plots are from a set of empirical relationships derived by Roth (2007) from a compilation of observational data, which is one of the few comprehensive data sources available for the mixed layer over an urban area. The curves follow the empirical relationships:

$$
\begin{aligned}
I_u &= 0.259 + 0.582 \exp\left[-0.943(z/z_H)\right] \\
I_v &= 0.163 + 0.391 \exp\left[-0.563(z/z_H)\right] \\
I_w &= 0.114 + 0.226 \exp\left[-0.634(z/z_H)\right]
\end{aligned} \tag{1}
$$

where z/z_H represents the ratio of observation height to area-averaged building height. The data used to construct these relationships was gathered over a variety of urban and suburban surfaces, and is gathered from periods of neutral stability ($|\zeta| < 0.1$). The figure shows that during all stability intervals, the data observed over New York City at 3 different sites aligns well with the empirical curves in all directions in the lower levels of the boundary layer. The most significant outlier is the lowest level measurement at Manhattan ($z/z_H \backsim 2$), which is significantly higher than the curve value at the same height. This outlier may be caused by the placement of the observational instrument in the surface layer, where the effects of high roughness elements lead to high σ_j values. It is also worth noting that while the point might be above the urban canopy layer, it is in the urban roughness layer due to large values of z_H in Manhattan. The value at $z/z_H \backsim 2$ follows the curve at moderately stable period and difference increases as instability increases. Similarly during the very stable period the value is high, which may be due to intermittency in turbulence during nighttime and early morning hours (Frehlich et al. 2006; Mahrt 1998).

3.3 Velocity Spectra

Figure 8 shows the mixed layer spectra of w over the Manhattan site for various surface layer stabilities. While the spectra were computed using data obtained from the Doppler lidar, they were binned based on different ζ values calculated using sonic anemometer as described in Sect. 2.3.2. The x-axis of the spectra represents the frequency (f) normalized by measurement height (z) and horizontal wind speed averaged over 30 min periods ($\overline{U}$), while the y-axis represents the spectral energy density normalized by f and $\overline{U}^2$. The different colors indicate different measurement heights (Fig. 7).

The spectra show 2 different turbulence regimes for most stability intervals: one in the lower 500 m and another above 1000 m. Except during the highly stable period, all other spectra exhibit a traditional hump-shaped curve. Additionally, the lidar is able to recover the -5/3 Kolmogorov curve in the inertial subrange regardless of surface stability and height, which suggests that the subrange is well-resolved by the 1 Hz temporal resolution (Beare 2014; Davidson 2015). In general, the energy contained in the lower levels of the mixed layer at 200, 300, and 500 m is higher compared to 1000 m and 1500 m, which represents the strength of near-surface strong buoyancy and shear. The normalized peak frequencies observed at all heights are similar. During unstable periods ($\zeta < -0.1$) the spectral curves from 200 to 500 m are identical, and similarly, the 1000 & 1500 m curves are alike. As the boundary layer becomes unstable, there is higher stratification between vertical levels, as shown by a shift in peak normalized frequency (fz/U), suggesting decoupling between the lower and upper portions of the mixed layer. This behavior is also evident during the neutral period, which is expected. During the stable period ($0.1 \leq \zeta < 0.5$), the spectra collapse on each other with no discernible behavior between heights. The frequencies of peak spectral energy for the unstable periods are approximately 0.4 and 0.1 for lower levels, respectively, while they increase to approximately 1 and 0.6 during the stable period, respectively. This shift may represent a transition from mixing driven by larger-scale convective structures during periods of surface instability (buoyancy) to eddies generated by horizontal winds during periods of surface stability (shear) (Nordbo 2013).

During unstable periods, the lower mixed layer ($z < 500$ m) spectra observed in the mixed layer over Manhattan follow similar profiles and trends with regards to stability to those reported by other studies in the urban surface layer (Nordbo 2013; Ramamurthy and Eric 2015; Roth et al. 2015). The vertical stratification may be a result of a combination of thermal and mechanical turbulence being stronger at low-levels, with buoyant and shear-induced mixing being strongest within the local internal boundary layer and decaying with increasing height into the upper mixed layer. This behavior suggests that surface properties influence turbulent characteristics throughout the mixed layer due to contributions from buoyancy-generated turbulence (from large surface heat fluxes due to high fractions of impervious surface cover (Oke 1995)) and shear-generated turbulence (due to large building heights). This phenomenon can be seen by the similar spectral energy densities at lower levels relative to those at higher levels. During slightly stable periods, spectra show that the UBL is dominated by shear with little to no influence from buoyancy, as evidenced by the similarity in energy densities between the lower and upper mixed layer spectra. During this period, all the levels are likely in the residual layer. During highly stable periods, the dissimilarity between energy densities at lower and upper mixed layer levels becomes apparent again, which suggests that localized and intermittent shear becomes dominant, especially as values of U increase, resulting in sporadically yet strong disorganized turbulence (Anisimov 2013).

3.4 Normalized Standard Deviations and Variances of Wind Components

In order to further analyze the coupling between the surface and mixed layer during periods of surface instability, normalized standard deviations of w were analyzed at different levels in the UBL. The results from this analysis were compared with similar analyses (see Table 4) performed in different studies to investigate the validity of surface layer scaling for vertical mixing in the mixed layer.

To evaluate $\sigma_w/u*$ during periods of surface instability, observations were filtered to $\zeta < -0.1$ with turbulent heat flux values $\overline{w'T'} > 0.01 K\,\mathrm{ms}^{-1}$, as performed in Wood et al. (2010). This filtering attempts to remove noisy data and improve the ability of the empirical curves to improve the representation of convective processes. To establish a correlation between ζ and $\sigma_w/u*$, the relationship formulated in Panofsky et al. (1997) is used:

$$\sigma_j/u_* = a_j(1 - b_j\zeta)^c, \tag{2}$$

where a_j and b_j are empirical coefficients, whereas typically $c = 1/3$ for unstable conditions. Figure 9 shows the normalized standard deviations of vertical velocities, where standard deviations of w are (σ_w) normalized by surface friction velocity, u_*, at the Queens and Staten Island sites at heights representative of the lower and upper mixed layer (200 and 1000 m a.g.l., respectively). The Manhattan site was excluded due to an insufficient sample size for this analysis after data filtering. The 200 m level was selected such that a z/z_H value would be similar to those in the studies references listed in Table 4, allowing for a direct comparison between the analysis herein and the studies. The 1000 m level was selected to evaluate the relationship of σ_w/u_* and ζ to determine the impact of the surface layer on the upper mixed layer at a height not observed before, to the authors' knowledge.

In general, the profiles of σ_w/u_* exhibit a similar relationship to similar studies in other cities, albeit at lower magnitudes with increasing height. In the lower mixed layer (measurement height of 200 m a.g.l.), the profiles for Queens and Staten Island both show strong agreement with other studies, with a_w of 0.86 and 0.50, respectively, and b_w of 5.45 and 22.8, respectively. This agreement shows the similarity of vertical boundary layer turbulence

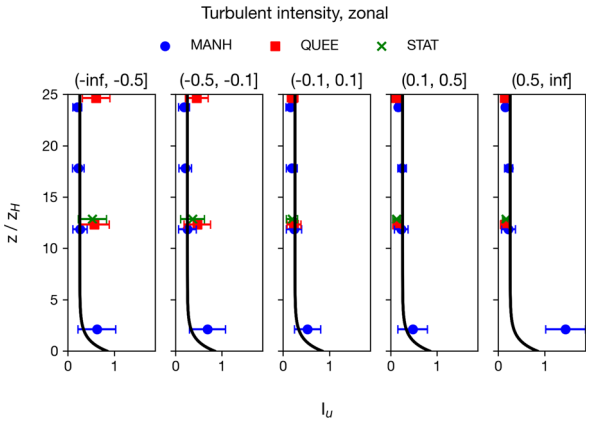

(a)

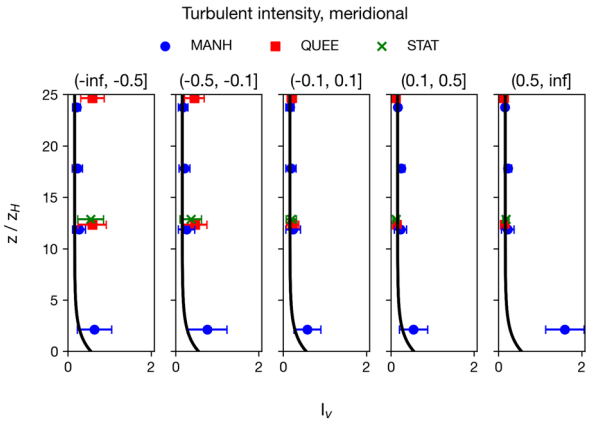

(b)

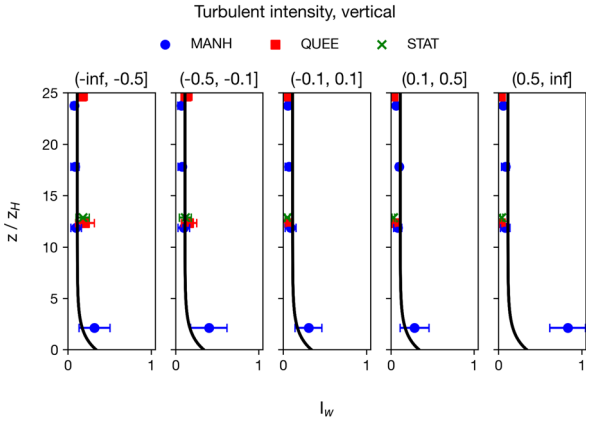

(c)

Fig. 7 Comparison of turbulent intensity profiles with empirical relationships derived in Roth (2007) in the **a** zonal, **b** meridional, and **c** vertical directions for the lower mixed layer, grouped by stability. Error bars show $\pm 2 - \sigma$ from the mean over the observation period

Table 4 Normalized standard deviation fit coefficients for w at different normalized heights, z/z_H

Study	Code	Measurement height (m a.g.l.)	z/z_H	a_w	b_w	c_w
Queens	–	200	7.81	0.86	5.45	0.33
Queens	–	1000	39.0	0.61	1.33	0.33
Staten Island	–	200	21.4	0.50	22.8	0.33
Staten Island	–	1000	107	0.33	30.2	0.33
Wood et al. (2010)	W10	190	16.1	1.31	0.65	0.33
Quan and Fei (2009b)	Q09	325	5.42	1.33	1.27	0.33
Ramamurthy and Eric (2015)	R15	40	6.15	1.09	1.58	0.30
Roth (2007)	R00	–	2.50	1.12	2.48	0.33
Liu et al. (2017)	L17a	47	2.28	1.19	0.81	0.33
	L17b	140	6.80	1.21	0.76	0.33
	L17c	280	13.6	1.30	0.49	0.33
Fortuniak et al. (2013)	F13a	37	3.24	1.11	0.61	0.54
	F13b	42	2.63	1.21	0.88	0.43

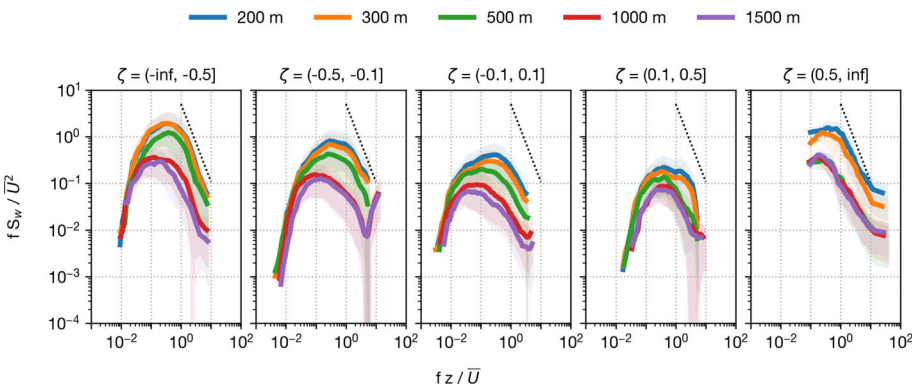

Fig. 8 Normalized power spectra for w at the Manhattan (MANH) observation site, averaged over stability group. Shading indicates $\pm$ 2-σ from the mean over the observation period. The $-$ 5/3 Kolmogorov curve is shown as the dotted black line

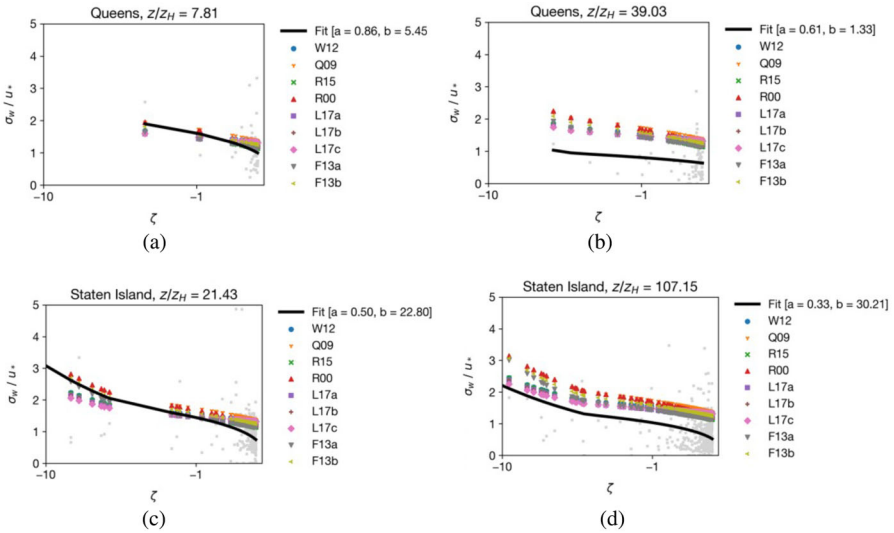

Fig. 9 Comparison of normalized standard deviation of vertical velocity, $\sigma_w/u*$, for Queens and Staten Island with studies referenced in Table 4 at 200 m a.g.l and 1000 m a.g.l., respectively. Grey dots represent 30 min data points from study sites

over different sites in New York City to other urban areas, as well as the validity of lidar for resolving these processes with some degree of accuracy compared to higher-frequency sonic anemometer data. In the upper mixed layer (measurement height of 1000 m a.g.l.), the profiles for both sites demonstrate similar relationships between σ_w/u_* and ζ to those at lower heights in other studies, although with significantly lower magnitude of σ_w/u_*. The lower magnitudes indicate that vertical mixing at this height is weaker than in the lower mixed layer, which is expected. However, the similarity in profiles demonstrates that upper mixed layer vertical mixing, represented by σ_w, exhibit dependence on surface layer processes, represented by u_*.

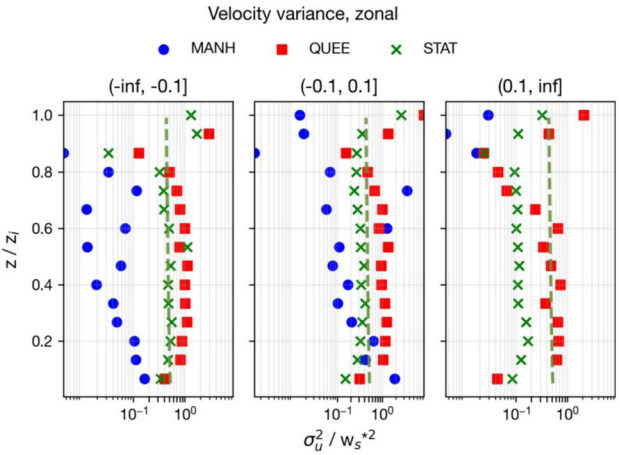

Fig. 10 Variance of zonal winds normalized by convective velocity, $w*$, compared to observations from Lenschow et al. (1980) (shown as the green dashed line)

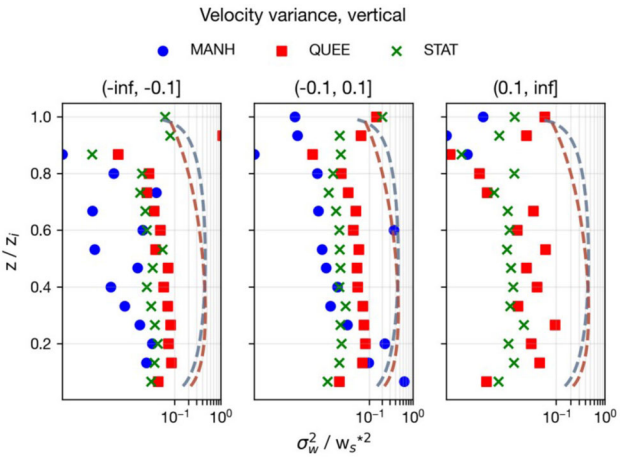

Fig. 11 Variance of vertical velocities normalized by convective velocity, $w*$, compared to observations from Lenschow et al. (1980) (red dashed line) and Sorbjan (1986) (grey dashed line)

Vertical profiles of velocity variances normalized by the convective velocity scale (w_s*) (Deardorff et al. 1970) were evaluated at all sites to observe the validity of convective scaling for velocity variances in the UBL. The w_s*-normalized zonal and vertical variances are shown in Figs. 10 and 11. Based on observational data, scaling for zonal wind variances (σ_u^2/w_s*) showed similar profiles to those in Lenschow et al. (1980) for Queens and Staten Island, with significantly lower values in Manhattan during unstable periods. This is similar to the vertical wind variances (σ_w^2/w_s*), where all sites feature lower magnitudes of scaled variances, albeit sharing similar profiles to those provided in Lenschow et al. (1980) and Sorbjan (1986). The differences in scaled values suggest several causes, but the primary causes are hypothesized to be (1) improper temporal resolution and sample size of observational data, and (2) values of w_s* significantly higher than those in the referenced studies. With regards to improper temporal resolution, the referenced studies recorded data at 20 Hz (Lenschow et al. 1980)

and 10 Hz (Izumi and James 1976), which resolve winds at far higher resolutions than those captured by lidar data (1 Hz maximum). Additionally, the sample size for Manhattan data may be inadequate to properly characterize the full range of velocities over the site (these limitations are discussed further in Sect. 4. With regards to the magnitudes of w_s*, the values over the observation period were 2.87 ± 1.26 ms^{-1} at the Manhattan observation site, 1.37 ± 0.78 ms^{-1} at Queens, and 1.47 ± 0.77 ms^{-1} at Staten Island. The magnitude of the values at the Manhattan site exceeds maximum values from Lenschow et al. (1980) (2.51 ms^{-1}), which may decrease the scaled value further from the reference curve.

4 Conclusions

The observations and analysis shown in this paper provide new insight into characteristics of boundary layer turbulence over urban areas, with an emphasis on the use of lidar for observing UBL dynamics throughout the mixed layer at multiple locations within a city. These results allow for the motivating questions to be addressed:

1. In general, vertical profiles of turbulence in the urban boundary layer show high magnitudes of turbulent properties (such as I_j) near the surface and decreasing magnitudes with increasing height, which is expected. The rate of decrease with height, however, is dependent on atmospheric stability, as turbulent properties demonstrate lower vertical gradients with decreasing atmospheric stability, indicating strong vertical mixing throughout the UBL. This behavior is shown to be similar at each observation site, which implies a degree of homogeneity in the boundary layer over New York City despite a highly heterogeneous surface layer. Grouping observations and analysis by stability regimes reveal the dependence of turbulent properties on atmospheric stability, with decreasing turbulence with increased surface stability, which is also expected. During periods of high instability ($\zeta < -0.1$), mean turbulent intensities (I_j) show little dependence on height, which also implies strong vertical mixing through the mixed layer. In contrast, height dependence increases with increasing ζ, where values of I_j assume profiles more similar to the classic logarithmic shape characteristic of boundary layer properties. With regards to spectral properties of boundary layer turbulence, vertical stratification in turbulent processes throughout in the mixed layer becomes evident during periods of strong atmospheric instability, with distinct differences in spectral energy and peak normalized frequencies the lower mixed layer (≤ 500 m) and the upper mixed layer (≥ 1000 m). This may highlight the decoupling between the surface and mixed layers and the dominance of buoyancy-driven flows (i.e., thermals) in turbulent mixing throughout the lower mixed layer, whereas shear-generated turbulence dominates closer to the boundary layer height.
2. Vertical profiles of mixed layer turbulence appear to be homogeneous throughout New York City, based on observations and analysis from the sites used for this study. Magnitudes of winds and turbulent properties vary between sites at lower levels, with near-surface values higher in Manhattan than Queens or Staten Island, but becoming increasingly similar with height. Wind directions are especially evident of this trend, with Manhattan demonstrating markedly different 200 m wind direction distributions than Queens and Staten Island (southerly versus west-southwesterly), but demonstrating a shift in direction with height (increasingly west-southwesterly), which align with the wind directions in others sites. In spite of these differences, vertical profiles of these properties are similar between sites throughout the majority of the UBL, with differences becoming relatively small throughout the mixed layer. The exception to this occurs during

periods of atmospheric stability, in which we hypothesize that sporadic turbulence generated by localized shears increases I_j, which is observed for the Manhattan site. This implies horizontal homogeneity in turbulent properties, indicating that surface effects may be limited in horizontal distribution of properties of the UBL.

3. The mixed layer appears to depend on surface layer properties during periods of non-neutral atmospheric stability. Variability in spectra of vertical velocity with height show a dependence of turbulence on height, with the lower 500 m demonstrating similar spectral energy profiles over the range of resolved frequencies, while mixed layer spectral profiles (≥ 1000 m) were found to have similar peak normalized frequencies despite having lower energy densities, suggesting influence of the surface in the mixed layer. Analysis of σ_w/u_* also supports this dependence, as it shows that normalize variance values increase with decreasing ζ at different heights in the mixed layer. Although this result is not surprising, the similarity in the profile of σ_w/u_* in the deep mixed layer ($z = 1000$ m) is suggestive of the influence of surface layer properties throughout the entire mixed layer during unstable periods, implying that vertical mixing in the mixed layer is influenced by surface layer properties regardless of height. It is worth noting that the magnitudes of σ_w/u_* are lower in the upper mixed layer than the lower mixed layer, which is expected, as the strength of surface forcings (i.e., thermals, surface friction drag) decreases with increasing height. This relationship suggests that scaling arguments may be relevant and accurate throughout the entirety of the mixed layer.

Despite the extensive observational data available for this study, several opportunities exist to provide a more robust analysis of turbulence in the UBL. Chief among these are the availability of data at the Manhattan site, where the lack of lidar data at the site for the entire calendar year, as in Queens and Staten Island, removes a useful dataset from the analysis and hinders further analysis of spatial variability in the one of the most heavily urbanized neighborhoods in New York City. The incorporation of high-frequency temperature (T) and specific humidity (q) measurements would be an invaluable addition to the study of turbulent transports of heat and moisture through the mixed layer, as is frequently done in studies using eddy-covariance methods in the surface and inertial sublayers. This would also enable the classification of boundary layer stability regimes using the Richardson number rather than dependence of stability classification on surface conditions, which may be more appropriate for mixed layer stability classification due to the time required for surface layer properties to mix vertically (especially during transitional periods, as is common in the mornings). Additionally, the lack of < 1 Hz lidar data in the three wind directions at each site is an obstacle to resolving the highest frequency signals for turbulence throughout the mixed layer, which is a level of resolution afforded by many sonic anemometers, which allows for analysis at high temporal resolutions to occur at the lowest levels of the boundary layer. In addition to additional remotely-sensed data, the incorporation of observations at ground level would allow for the observation of the entire UBL. With regards to the analyses performed herein, this might improve the accuracy of derived quantities relevant for scaling purposes, such as w_*. This would facilitate the analysis of interactions between the surface and mixed layer, which supports the investigation of the applicability (or lack thereof) of Monin-Obukhov similarity theory to the UBL (Pelliccioni et al. 2012; Theeuwes et al. 2019). This question has relevant implications, due to the widespread use of Monin-Obukhov similarity theory in numerical weather prediction models. This is especially important, as there is a need for improved representation and forecasting of atmospheric processes at smaller scales over heterogeneous terrain, such as cities (Ronda et al. 2017; Baklanov 2018).

Acknowledgements The authors would like to thank the editor and two anonymous reviewers, whose comments and suggestions have helped improved the quality of this manuscript. This study is supported and monitored by The National Oceanic and Atmospheric Administration—Cooperative Science Center for Earth System Sciences and Remote Sensing Technologies (NOAA-CESSRST) under the Cooperative Agreement Grant NA16SEC4810008. The authors would like to thank The City College of New York, the NOAA-CESSRST program, and the NOAA Office of Education, Educational Partnership Program for fellowship support for Gabriel Rios. The statements contained within the manuscript/research article are not the opinions of the funding agency or the U.S. government, but reflect the author's opinions. This research is also made possible by the New York State (NYS) Mesonet. Original funding for the NYS Mesonet was provided by Federal Emergency Management Agency grant FEMA-4085-DR-NY, with the continued support of the NYS Division of Homeland Security & Emergency Services; the state of New York; the Research Foundation for the State University of New York (SUNY); the University at Albany, SUNY; the Atmospheric Sciences Research Center (ASRC) at SUNY Albany; and the Department of Atmospheric and Environmental Sciences (DAES) at SUNY Albany. This research was also funded by the Department of Defense Army Research Office Grant No. W911NF2020126.

References

Anisimov SV et al (2013) Aeroelectric structures and turbulence in the atmospheric boundary layer. Nonlinear Process Geophys 20(5):819–824

Baklanov AA et al (2011) The nature, theory, and modeling of atmospheric planetary boundary layers. Bull Am Meteorol Soc 92(2):123–128. https://doi.org/10.1175/2010BAMS2797.1

Baklanov A et al (2018) From urban meteorology, climate and environment research to integrated city services. Urban Clim 23:330–341

Banks RF et al (2015) Performance evaluation of the boundary-layer height from lidar and the Weather Research and Forecasting model at an urban coastal site in the north-east Iberian Peninsula. Boundary-Layer Meteorol 157(2):265–292

Barlow JF (2014) Progress in observing and modelling the urban boundary layer. Urban Clim 10:216–240. https://doi.org/10.1016/j.uclim.2014.03.011

Barlow JF et al (2011) Boundary layer dynamics over London, UK, as observed using Doppler lidar during REPARTEE-II. Atmos Chem Phys 11(5):2111–2125. https://doi.org/10.5194/acp-11-2111-2011

Beare Robert J (2014) A length scale defining partially-resolved boundary layer turbulence simulations. Boundary-Layer Meteorol 151:39–55

Calmet I, Mestayer P (2016) Study of the thermal internal boundary layer during sea-breeze events in the complex coastal area of Marseille. Theor Appl Climatol 123(3):801–826

Castillo MC, Inagaki A, Kanda M (2011) The effects of inner- and outer-layer turbulence in a convective boundary layer on the near-neutral inertial sublayer over an urban-like Sur690 face. Boundary-Layer Meteorol 140(3):453–469. https://doi.org/10.1007/s10546-011-9614-4

Cheynet E, Jakobsen JB, Reuder J (2018) Velocity spectra and coherence estimates in the marine atmospheric Bound695 ary layer. Boundary-Layer Meteorol 169(3):429–460. https://doi.org/10.1007/s10546-018-0382-2

Collier CG et al (2005) Dual-Doppler lidar measurements for improving dispersion models. Bull Am Meteorol Soc 86(6):825–838. https://doi.org/10.1175/BAMS-86-6-825

Davidson Peter Alan (2015) Turbulence: an introduction for scientists and engineers. Oxford University Press

Deardorff JW et al (1970) Convective velocity and temperature scales for the unstable planetary boundary layer and for Rayleigh convection. J Atmos Sci 27(8):1211–1213

Delgado Ruben et al (2015) Elastic lidar measurements of summer noctur710 nal low level jet events over Baltimore, Maryland. J Atmos Chem 72(3):311–333

Feigenwinter C, Vogt R, Parlow E (1999) Vertical Structure of Selected Turbulence Characteristics above an Urban Canopy. Theor Appl Climatol 62(1–2):51–63. https://doi.org/10.1007/s007040050074

Foken T et al (2004) Post-field data quality control. In: Handbook of Micrometeorology, p 28

Fortuniak K, Pawlak WL, Siedlecki M (2013) Integral turbulence statistics over a central European city centre. Boundary-Layer Meteorol 146(2):257–276

Frehlich R et al (2006) Measurements of boundary layer profiles in an urban environment. J Appl Meteorol Climatol 45(6):821–837

Garratt JR (1990) The internal boundary layer—a review. Boundary-Layer Meteorol 50(1–4):171–203. https://doi.org/10.1007/BF00120524

Garratt J (1994) Review: the atmospheric boundary layer. Earth Sci Rev 37(1):89–134. https://doi.org/10.1016/0012-8252(94)90026-4
Godowitch JM, Ching JKS, Clarke JF (1987) Spatial variation of the evolution and structure of the urban boundary layer. Boundary-Layer Meteorol 38(3):249–272
Grachev AA et al (2013) The critical Richardson number and limits of applicability of local similarity theory in the stable boundary layer. Boundary-Layer Meteorol 147(1):51–82
Granados-Muñoz MJ et al (2012) Automatic determination of the planetary boundary layer height using lidar: one-year analysis over southeastern Spain. J Geophys Res Atmos 117(D18)
Halios CH, Janet FB (2018) Observations of the morning development of the urban boundary layer over London, UK, taken during the ACTUAL project. Boundary-Layer Meteorol 166(3):395–422
Haman CL, Lefer B, Morris GA (2012) Seasonal variability in the diurnal evolution of the boundary layer in a near-coastal 20 Gabriel Rios, Prathap Ramamurthy urban environment. J Atmos Ocean Technol 29(5):697–710
Hanna S, White J, Zhou Y (2007) Observed winds, turbulence, and dispersion in built-up downtown areas of Oklahoma City and Manhattan. Boundary-Layer Meteorol 125(3):441–468. https://doi.org/10.1007/s10546-007-9197-2
Hildebrand PH, Ackerman B (1984) Urban effects on the convective boundary layer. J Atmos Sci 41(1):76–91. https://doi.org/10.1175/1520-0469(1984)041<0076:UEOTCB>2.0.CO;2
Hogan RJ et al (2009) Vertical velocity variance and skewness in clear and cloud-topped boundary layers as revealed by Doppler lidar: vertical velocities from Doppler lidar. Q J R Meteorol Soc 135(640):635–643. https://doi.org/10.1002/qj.413
Izumi Y, Caughey JS (1976) Minnesota 1973 atmospheric boundary layer experiment data report. vol 76. 38. Air Force Cambridge Research Laboratories, Air Force Systems Command, United States Air Force
Kaimal JC, Finnigan JJ (1994) Atmospheric boundary layer flows: their structure and measurement. Oxford University Press
Kastner-Klein P, Rotach MW (2004) Mean flow and turbulence characteristics in an urban roughness sublayer. Boundary-Layer Meteorol 111(1):55–84. https://doi.org/10.1023/B:BOUN.0000010994.32240.b1
Klein PM, Hu X-M, Xue M (2014) Impacts of mixing processes in nocturnal atmospheric boundary layer on urban ozone concentrations. Boundary-Layer Meteorol 150(1):107–130. https://doi.org/10.1007/s10546-013-9864-4
Kotthaus S et al (2018) Volume for pollution dispersion: London's atmospheric boundary layer during ClearfLo observed with two ground-based lidar types. Atmos Environ 190:401–414. https://doi.org/10.1016/j.atmosenv.2018.06.042
Kumer V-M, Reuder J, Furevik BR (2014) A comparison of LiDAR and radiosonde wind measurements. Energy Procedia 53:214–220. https://doi.org/10.1016/j.egypro.2014.07.230
Lenschow DH, Wyngaard JC, Pennell WT (1980) Mean-field and second-moment budgets in a baroclinic, convective boundary layer. J Atmos Sci 37(6):1313–1326. https://doi.org/10.1175/1520-0469(1980)037<1313MFASMB>2.0.CO;2
Liu Y, Liu H, Wang L (2017) The vertical distribution characteristics of integral turbulence statistics in the atmospheric boundary layer over an urban area in Beijing. Sci China Earth Sci 60(8):1533–1545
Macdonald RW (2000) Modelling the mean velocity profile in the urban canopy layer. Boundary-Layer Meteorol 97(1):25–45. https://doi.org/10.1023/A:1002785830512
Mahrt L (1998) Nocturnal boundary-layer regimes. Boundary-layer Meteorol 88(2):255–278
Melecio-Vázquez D et al (2018) Thermal structure of a coastal-urban boundary layer. Boundary-Layer Meteorol 169(1):151–161. https://doi.org/10.1007/s10546-018-0361-7
Mestayer PG et al (2005) The urban boundary-layer field campaign in Marseille (UBL/CLU-ESCOMPTE): set-up and first results. Boundary-Layer Meteorol 114(2):315–365
Morss RE et al (2011) Improving societal outcomes of extreme weather in a changing climate: an integrated perspective. Annu Rev Environ Resour 36:1–25
National Research Council et al (2012) Urban meteorology: forecasting, monitoring, and meeting users' needs, National Academies Press
Newsom RK et al (2005) Retrieval of microscale wind and temperature fields from single- and Dual-Doppler lidar data. J Appl Meteorol 44(9):1324–1345. https://doi.org/10.1175/JAM2280.1
Nordbo A et al (2013) Intra-city variation in urban morphology and turbulence structure in Helsinki, Finland. Boundary-Layer Meteorol 146(3):469–496. https://doi.org/10.1007/s10546-012-9773-y
NYC Department of City Planning (2023) Residence Districts Zoning Data Tables. https://www.nyc.gov/assets/planning/download/pdf/zoning/districts-tools/residencespszoningspsdataspstables.pdf
Oke TR (1995) The heat island of the urban boundary layer: characteristics, causes and effects. In: Wind climate in cities, pp 81-107

Pal S et al (2012) Spatio-temporal variability of the atmospheric boundary layer depth over the Paris agglomeration: an assessment of the impact of 22 Gabriel Rios, Prathap Ramamurthy the urban heat island intensity. Atmos Environ 63:261–275
Panofsky HA et al (1977) The characteristics of turbulent velocity components in the surface layer under convective conditions. Boundary-Layer Meteorol 11(3):355–361
Pelliccioni A et al (2012) Some characteristics of the urban boundary layer above Rome, Italy, and applicability of Monin-Obukhov similarity. Environ Fluid Mech 12(5):405–428
Petäjä T et al (2016) Enhanced air pollution via aerosol-boundary layer feedback in China. Sci Rep 6(1):1–6
Quan L, Hu F (2009) Relationship between turbulent flux and variance in the urban canopy. Meteorol Atmos Phys 104(1–2):29–36. https://doi.org/10.1007/s00703-008-0012-5
Quan L, Hu F (2009) Relationship between turbulent flux and variance in the urban canopy. Meteorol Atmos Phys 104(1):29–36
Ramamurthy P, Pardyjak ER (2015) Turbulent transport of carbon dioxide over a highly vegetated suburban neighbourhood. Boundary-Layer Meteorol 157(3):461–479
Ronda RJ et al (2017) Urban finescale forecasting reveals weather conditions with unprecedented detail. Bull Am Meteorol Soc 98(12):2675–2688
Rotach MW (1999) On the influence of the urban roughness sublayer on turbulence and dispersion. Atmos Environ 8
Roth M (1993) Turbulent transfer relationships over an urban surface. II: Integral statistics. Q J R Meteorol Soc 119(513):1105–1120. https://doi.org/10.1002/qj.49711951312
Roth M (2000) Review of atmospheric turbulence over cities. Q J R Meteorol Soc 126(564):941–990. https://doi.org/10.1002/qj.49712656409
Roth M, Oke TR (1993) Turbulent transfer relationships over an urban surface. I. Spectral characteristics. Q J R Meteorol Soc 119(513):1071–1104. https://doi.org/10.1002/qj.49711951311
Roth M et al (2015) Small-scale spatial variability of turbulence statistics,(co) spectra and turbulent kinetic energy measured over a regular array of cube roughness. Environ Fluid Mech 15(2):329–348
Shrestha B et al (2021) Overview and applications of the New York State mesonet profiler network. J Appl Meteorol Climatol. https://doi.org/10.1175/JAMCTurbulence
Sorbjan Z (1986) On similarity in the atmospheric boundary layer. Boundary-Layer Meteorol 34(4):377–397. https://doi.org/10.1007/BF00120989
Stull RB (1988) An introduction to boundary layer meteorology. vol 13. Springer
Sullivan John T et al (2017) Lidar observations revealing transport of O3 in the presence of a nocturnal low-level jet: regional implications for nextday pollution. Atmos Environ 158:160–171
Theeuwes NE et al (2019) Parametrizing horizontally-averaged wind and temperature profiles in the urban roughness sublayer. Boundary-Layer Meteorol 173(3):321–348
Verkaik JW, Holtslag AAM (2007) Wind profiles, momentum fluxes and roughness lengths at Cabauw revisited. Boundary-Layer Meteorol 122:701–719
Wang L et al (2014) Turbulent transport of momentum and scalars above an urban canopy. Boundary-Layer Meteorol 150(3):485–511. https://doi.org/10.1007/s10546-013-9877-z
Wang C et al (2016) Measuring boundary-layer height under clear and cloudy conditions using three instruments. Particuology 28:15–21. https://doi.org/10.1016/j.partic.2015.04.004
Wood CR et al (2010) Turbulent flow at 190 m height above London during 2006–2008: a climatology and the applicability of similarity theory. Boundary-Layer Meteorol 137(1):77–96. https://doi.org/10.1007/s10546-010-9516-x
Zhang D-L, Zhang S, Weaver SJ (2006) Low-level jets over the mid-Atlantic states: warm-season climatology and a case study. J Appl Meteorol Climatol 45(1):194–209